Article

Kinetics and Mechanism of the General-Acid-Catalyzed Ring-Closure of the Malondialdehyde–DNA Adduct, *N*-(3-Oxo-1-propenyl)deoxyguanosine (*N*OPdG), to 3-(2‘-Deoxy-β-d-*erythro*-pentofuranosyl)pyrimido[1,2-□]purin- 10(3*H*)-one (MdG)

James N. Riggins, Derek A. Pratt, Markus Voehler, J. Scott Daniels, and Lawrence J. Marnett

J. Am. Chem. Soc., **2004**, 126 (34), 10571-10581• DOI: 10.1021/ja040010q • Publication Date (Web): 24 July 2004

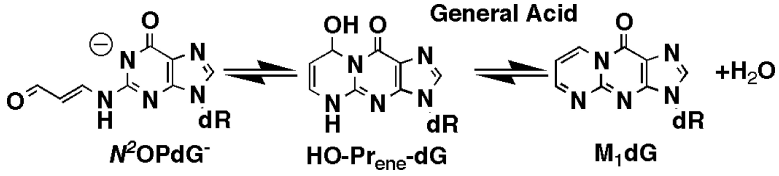

More About This Article

Additional resources and features associated with this article are available within the HTML version:

- Supporting Information
- Links to the 8 articles that cite this article, as of the time of this article download
- Access to high resolution figures
- Links to articles and content related to this article
- Copyright permission to reproduce figures and/or text from this article

View the Full Text HTML

J|A|C|S
ARTICLES
Published on Web 07/24/2004

Kinetics and Mechanism of the General-Acid-Catalyzed Ring-Closure of the Malondialdehyde−DNA Adduct, N^2-(3-Oxo-1-propenyl)deoxyguanosine (N^2OPdG$^-$), to 3-(2′-Deoxy-β-D-*erythro*-pentofuranosyl)pyrimido[1,2-α]purin-10(3*H*)-one (M_1dG)

James N. Riggins, Derek A. Pratt, Markus Voehler, J. Scott Daniels, and Lawrence J. Marnett*

Contribution from the A. B. Hancock Jr. Memorial Laboratory for Cancer Research, Departments of Biochemistry and Chemistry, Vanderbilt Institute of Chemical Biology, Center in Molecular Toxicology, Vanderbilt-Ingram Cancer Center, Vanderbilt University School of Medicine, Nashville, Tennessee 37232

Received January 7, 2004; E-mail: larry.marnett@vanderbilt.edu

Abstract: 3-(2′-Deoxy-β-D-*erythro*-pentofuranosyl)pyrimido[1,2-α]purin-10(3*H*)-one (M_1dG) is the major product of the reaction of deoxyguanosine with malondialdehyde (MDA). M_1dG blocks replication by DNA polymerases in vitro and is mutagenic in vivo. M_1dG reacts with hydroxide to form the N^2-(3-oxo-1-propenyl)-deoxyguanosine anion (N^2OPdG$^-$). This reaction is pH-dependent and reverses under neutral and acidic conditions to form M_1dG. Here we describe the kinetics and mechanism of the ring-closure reaction in both the nucleoside and oligonucleotides. Kinetic analysis of absorbance and fluorescence changes demonstrates that ring-closure is biphasic, leading to the rapid formation of an intermediate that slowly converts to M_1dG in a general-acid-catalyzed reaction. The dependence of the rate of the rapid phase on pH reveals the pK_a for protonated N^2OPdG is 6.9. One-dimensional ^{1}H NMR and DQF-COSY experiments identified two distinct intermediates, N^2OPdG-H and 8-hydroxy-6,7-propenodeoxyguanosine (HO-Pr$_{ene}$-dG), that are formed upon acidification of N^2OPdG$^-$. Characterization of ring-closure in single-stranded and in melted duplex oligonucleotides shows M_1dG formation is also acid-catalyzed in single-stranded oligonucleotides and that the denaturation of an oligonucleotide duplex enhances ring-closure. This work details the complexity of ring-closure in the nucleoside and oligonucleotides and provides new insight into the role of duplex DNA in catalyzing ring-opening and ring-closing of M_1dG and N^2OPdG.

Introduction

Oxygenation of cellular molecules such as DNA and lipids often leads to the formation of potent electrophiles capable of inducing oxidative damage and disease.[1−3] Within this group of reactive intermediates are the α,β-unsaturated aldehydes, a class of alkylating agents that have been shown to cause damage and subsequent mutations to DNA. Malondialdehyde (MDA) and related β-substituted acroleins have been shown by this and other laboratories to elicit the formation of various DNA adducts.[4,5] The most abundant DNA adduct derived from MDA is 3-(2′-deoxy-β-D-*erythro*-pentofuranosyl)pyrimido[1,2-α]purin-10(3*H*)-one (M_1dG).[6] M_1dG exists in duplex DNA as the ring-opened derivative, N^2-(3-oxo-1-propenyl)deoxyguanosine (N^2OPdG).

We recently described the kinetics and mechanism of ring-opening of M_1dG under basic conditions.[7] Ring-opening involves the reversible second-order addition of hydroxide to form the anion of N^2OPdG$^-$ (eq 1). Loss of hydroxide and cyclization to M_1dG is slow under basic conditions. The rate of cyclization to M_1dG is dramatically accelerated under acid conditions.

$$M_1\text{dG} + \text{OH}^- \rightleftharpoons N^2\text{OPdG}^- \quad (1)$$

Here we describe the kinetics and mechanism of ring-closure of N^2OPdG$^-$ to M_1dG as the nucleoside and in oligonucleotides. Ring-closure is a general-acid-catalyzed process that occurs at both acidic and neutral pH (Figure 1). Kinetic analyses of adduct absorption and fluorescence of acidified N^2OPdG$^-$ reveal a biphasic conversion of N^2OPdG$^-$ to M_1dG. Following protonation of N^2OPdG$^-$, an intermediate is formed that slowly dehydrates to M_1dG. Dehydration is rate-limiting and subject to general-acid catalysis. NMR analysis identified the intermediate as 8-hydroxy-6,7-propenodeoxyguanosine (HO-Pr$_{ene}$-dG). DFT calculations suggested the formation of other intermediates between N^2OPdG$^-$ and HO-Pr$_{ene}$-dG. NMR analysis revealed

(1) Gupta, R. C.; Lutz, W. K. *Mutat. Res.* **1999**, *424*, 1−8.
(2) Farmer, P. B.; Shuker, D. E. *Mutat. Res.* **1999**, *424*, 275−286.
(3) Bartsch, H. *Mutat. Res.* **1996**, *340*, 67−79.
(4) Marnett, L. J. *IARC Sci. Publ.* **1999**, 17−27.
(5) Marnett, L. J.; Plastaras, J. P. *Trends Genet.* **2001**, *17*, 214−221.
(6) Reddy, G. R.; Marnett, L. J. *J. Am. Chem. Soc.* **1995**, *117*, 5007−5008.
(7) Riggins, J. N.; Daniels, J. S.; Rouzer, C. A.; Marnett, L. J. *J. Am. Chem. Soc.* **2004**, *126*, 8237−8243.

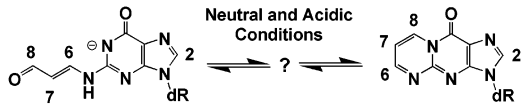

Figure 1. Ring-closure of N^2OPdG$^-$ occurs under neutral and acidic conditions. The numbering scheme for the MDA−DNA adduct in the ring-closure mechanism is shown.

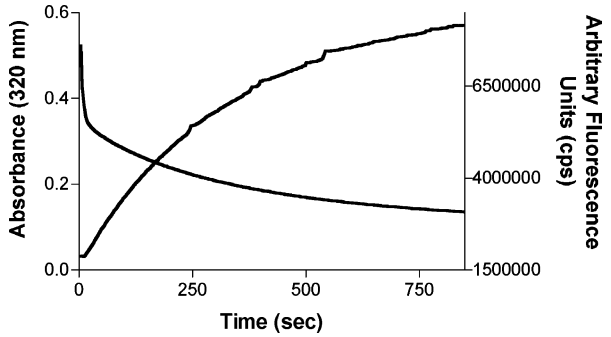

Figure 2. Time courses for changes in absorbance at 320 nm and fluorescence at 511 nm (excitation at 363 nm) following acidification of N^2OPdG$^-$. N^2OPdG$^-$ was combined with sodium phosphate, pH 4.7 at 25 °C, to a final concentration of 10^{-5} M and 0.45 M, respectively. Biphasic plots are observed in both absorbance and fluorescence measurements.

that denaturation of duplex DNA accelerates the rate of ring-closure of N^2OPdG$^-$ compared to N^2OPdG$^-$ in single-stranded DNA.

Results

Ring-Closure of N^2OPdG$^-$ is a Biphasic Process. The equilibrium between N^2OPdG$^-$ and M_1dG was probed under neutral and acidic conditions. The absorbance of N^2OPdG$^-$ at 320 nm and the fluorescence of M_1dG at 511 nm (excitation at 363 nm) were used to evaluate the kinetics of ring-closure. Figure 2 displays the change in absorbance and fluorescence of a solution of N^2OPdG$^-$ that has been acidified using phosphate buffer at pH 4.7. The change in both absorbance and fluorescence is biphasic, with a large decrease in absorbance at 320 nm occurring within the first few seconds following acidification. During this same period, the fluorescence did not change. Following the initial period, or fast phase, a slow decrease in absorbance occurred that corresponded to an increase in fluorescence. Figures 3 and 4 show the changes in the UV and fluorescence spectra for acidified N^2OPdG$^-$ in more detail.

The fast phase of ring-closure occurs immediately upon acidification and is completed under the conditions described in the Experimental Section within 5−10 s. Figure 3A and B show the rapid phase of ring-closure by absorbance and fluorescence, respectively. Interestingly, the extent of decrease in absorbance is a function of pH so that different plateaus are reached dependent on the final pH (Figure 3A). A maximal drop in absorbance is observed at or below pH 4.5. The fact that a plateau is reached in the absorbance decay plots indicates that acid is acting as a reactant and not as a catalyst (eq 2).

$$N^2\text{OPdG}^- + \text{H}_3\text{O}^+ \rightleftharpoons \text{H-Intermediate} + \text{H}_2\text{O} \qquad (2)$$

The absorbance data can be fit to a single-exponential decay to give k_{obsd} values for the fast phase or to linear functions to obtain initial rates (see Table 1). In contrast to the absorbance data, Figure 3B shows the rapid phase of ring-closure is marked by a period of minimal change in the total fluorescence of the

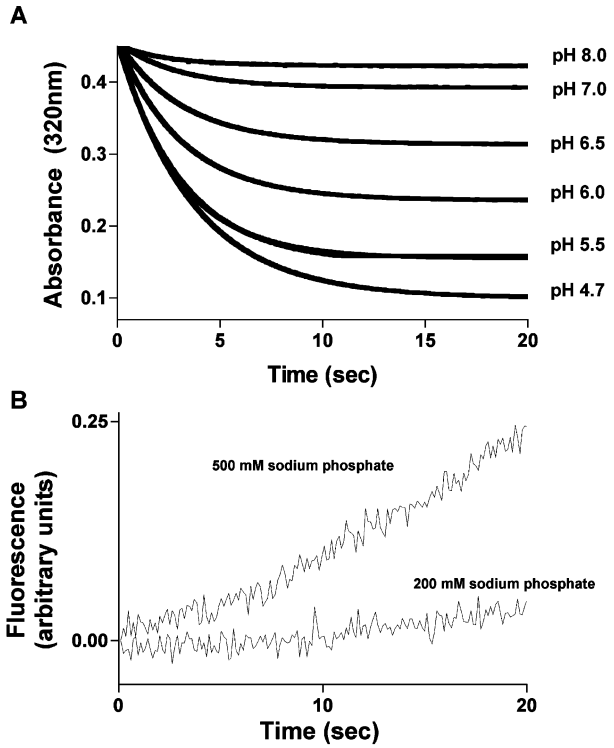

Figure 3. Kinetic plots reflecting the initial few seconds of ring-closure. Stopped-flow methods were used to observe changes in spectral properties for N^2OPdG$^-$: (A) absorbance at 320 nm and (B) fluorescence increase at 511 nm (excitation at 363 nm) upon rapid acidification. For absorbance decay experiments, N^2OPdG$^-$ (10^{-5} M final concentration) was combined with 0.5 or 0.2 M sodium phosphate buffers at various pH's at 25 °C. For fluorescence experiments, N^2OPdG$^-$ (10^{-5} M final concentration) was combined with 0.5 or 0.2 M sodium phosphate buffers at pH 4.7 at 25°C.

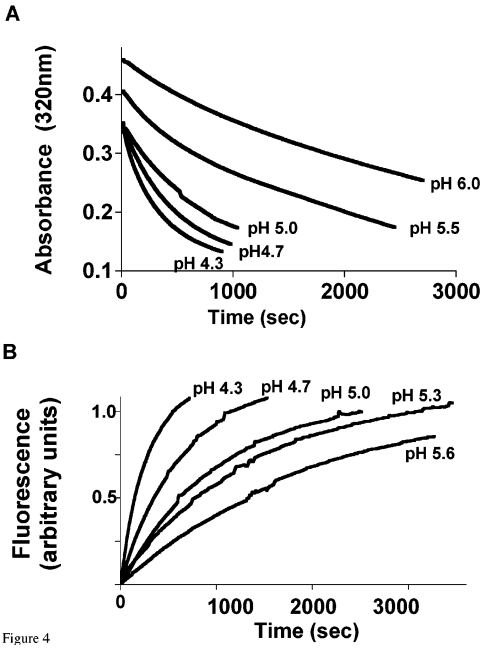

Figure 4

Figure 4. Kinetic decay plots for N^2OPdG$^-$ absorbance at 320 nm (A) and fluorescence increase at 511 nm (excitation at 363 nm) upon rapid acidification (B). N^2OPdG$^-$ (10^{-5} M final concentration) was combined with 0.5 or 0.2 M sodium phosphate buffers at various pH's at 25 °C.

solution. This observation of a lag phase implies little to no M_1dG is generated during the rapid phase of ring-closure and is the initial indication that a protonated intermediate is formed

Table 1. k_{obsd} (s^{-1}) for the Initial Phase of Ring-Closure Caused by Acid-Catalyzed N^2OPdG$^-$ Ring-Closure: Fast Phase in Sodium Phosphate at 25 °C

$[H_3O^+]$ (10^{-5} M)	k_{obsd} (s^{-1}) (250 mM sodium phosphate)	k_{obsd} (s^{-1}) (25 mM sodium phosphate)
32	0.109 ± 0.001	0.081 ± 0.002
10	0.106 ± 0.002	0.078 ± 0.002
3.2	0.055 ± 0.002	0.046 ± 0.001
1.0	0.029 ± 0.002	0.026 ± 0.001
0.3	0.015 ± 0.001	0.012 ± 0.001

Table 2. k_{obsd} Values Measured by Fluorescence Change for Acid-Catalyzed N^2OPdG$^-$ and N^2OPdG$^-$-Containing Oligonucleotide Ring-Closure: Slow Phase in 250 mM Sodium Phosphate at 25 °C

$[H_3O^+]$ (10^{-5} M)	$k_{obsd} \times 1000$ (s^{-1}) (N^2OPdG$^-$) absorbance	$k_{obsd} \times 1000$ (s^{-1}) (N^2OPdG$^-$) fluorescence	$k_{obsd} \times 1000$ (s^{-1}) (5′-A-X-A-3′) fluorescence	$k_{obsd} \times 1000$ (s^{-1}) (5′-T-X-T-3′) fluorescence
0.3	1.20 ± 0.1	1.30 ± 0.3	0.52 ± 0.1	0.52 ± 0.5
1.0	1.30 ± 0.1	1.44 ± 0.3	0.58 ± 0.1	0.59 ± 0.5
3.2	1.76 ± 0.1	2.04 ± 0.2	0.65 ± 0.1	0.72 ± 0.5
10	3.20 ± 0.1	3.35 ± 0.2	0.77 ± 0.1	1.07 ± 0.4
32	4.75 ± 0.2	6.22 ± 0.7	1.09 ± 0.3	1.43 ± 0.2
linear fit (r^2)	0.937	0.987	0.986	0.917

within seconds of acidification. The time scales for the fast phase probed by UV and fluorescence are equivalent, indicating they correspond to similar phenomena in solution. The rapid phase of ring-closure could be extended from 5 to 6 s to 10−12 s by cooling the reaction from ambient temperature to 8 °C (observed by fluorescence stopped-flow, Supporting Information 1).

Figure 4 shows the slow phase of ring-closure that takes place between the end of the fast phase and the end point of the reaction. Figure 4A shows ring-closure as a loss in the absorbance at 320 nm typical of the conversion of N^2OPdG$^-$ to M_1dG. The rate of absorbance decrease in the slow phase was dependent upon pH. Figure 4A also reveals that the starting point for absorbance decrease differed based on pH. This is consistent with the fact that the plateau reached for the fast phase of the reaction described in Figure 3A was pH-dependent. Nevertheless, the drop in absorbance for the slow phase arrives at a similar plateau regardless of pH or the plateau that was reached at the end of the fast phase (eq 3).

$$\text{H-Intermediate} \rightleftharpoons M_1dG + H_2O \quad (3)$$

This observation suggests that acid is acting as a catalyst in the slow phase. Experimental data were fit to a single-exponential decrease to obtain k_{obsd} values. Alternatively, the same set of experiments were completed by monitoring the formation of M_1dG as a function of fluorescence increase at 511 nm (Figure 4B), and data were analyzed as one-phase exponential increase functions. As seen in the absorbance decrease experiments above, the fluorescence increase also approached the same endpoint for the reaction regardless of the pH and the rate at which the reaction approached the endpoint was dependent on pH. The k_{obsd} values obtained through both absorbance decrease and fluorescence increase were similar in the range of H_3O^+ concentrations studied (Table 2), and a plot of k_{obsd} versus hydronium ion concentration gave a linear relationship (Figure 5).

Similar slow-phase studies were conducted for oligonucleotides bearing the N^2OPdG$^-$ adduct. Two sequence contexts were

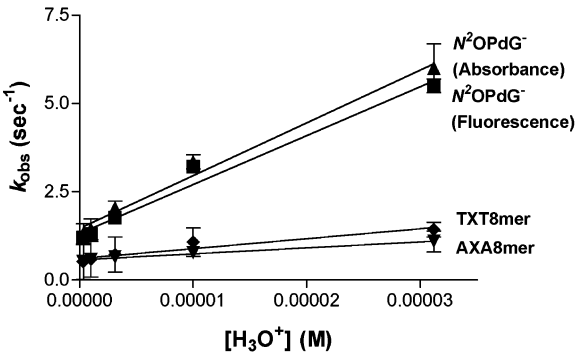

Figure 5. Plot of k_{obsd} vs $[H_3O^+]$. Triangles (▲) represent k_{obsd} determinations for the slow phase made using UV spectroscopy, and squares (■) represent k_{obsd} determinations for the slow phase made using fluorescence spectroscopy. Determinations of k_{obsd} for the slow phase with oligonucleotides 5′-A-X-A-3′ (▼) and 5′-T-X-T-3′ (◆), where X is N^2OPdG$^-$, were made using fluorescence spectroscopy.

used to evaluate if any difference in k_{obsd} could be observed for the adduct in oligonucleotides. Based on our previous study where ring-closure rate constants were affected by the sequence adjacent to the adduct site,[7] a purine flanking sequence (5′-GGA-N^2OPdG$^-$-ACCG-3′) and a pyrimidine flanking sequence (5′-GGT-N^2OPdG$^-$-TCCG-3′) were used. Data were collected using fluorescence increase as an indicator of M_1dG formation in oligonucleotides, and k_{obsd} values were determined by fitting the rate data to single-exponential increase functions. The kinetic data for ring-closure in nucleoside and oligonucleotides acquired using fluorescence increase are reported in Table 2. The k_{obsd} values determined for all pH values are reduced compared to the values determined for the nucleoside. Also, plots of k_{obsd} versus hydronium ion concentration yield linear fits (Figure 5). The pH-dependence in oligonucleotides is similar to that observed for the nucleoside but with a reduction in the ring-closure rate constant observed for all pH values.

Effect of Protonation on N^2OPdG$^-$ Stability. Earlier results indicate that M_1dG opens to form the N^2OPdG anion in basic solutions. The small reverse rate constants for M_1dG formation observed at basic pH (1.7×10^{-4} sec^{-1}), where N^2OPdG is deprotonated, imply that deprotonation has a stabilizing effect on the ring-opened adduct. This is supported by the fact that lowering the pH of a solution containing N^2OPdG$^-$ increases the k_{obsd} for ring-closure in both the fast and slow phases of the reaction (Tables 1 and 2).

Stopped-flow absorbance and fluorescence spectroscopy were used to determine the pK_a for N^2OPdG. Figure 6 displays the effect of acidifying N^2OPdG$^-$ on its absorbance at 320 nm. Though it is possible that the change in absorbance during the rapid phase is simply the result of protonation, the relatively long time scale observed for the rapid phase (5−10 s) suggests protonation is followed by a rapid transformation to an intermediate (eq 3). In this case,[8] eq 3 can be rewritten as

$$N^2\text{OPdG}^- + H_3O^+ \underset{K_a}{\rightleftharpoons} N^2\text{OPdG-H} + H_2O \rightleftharpoons \text{H-Intermediate} \quad (4)$$

Since the protonation is fast, the initial rates observed by absorbance decrease refer to the conversion of H-N^2OPdG to a

(8) Conners, K. A. *Chemical kinetics: the study of reaction rates in solution*; VCH Publishers: New York, 1990.

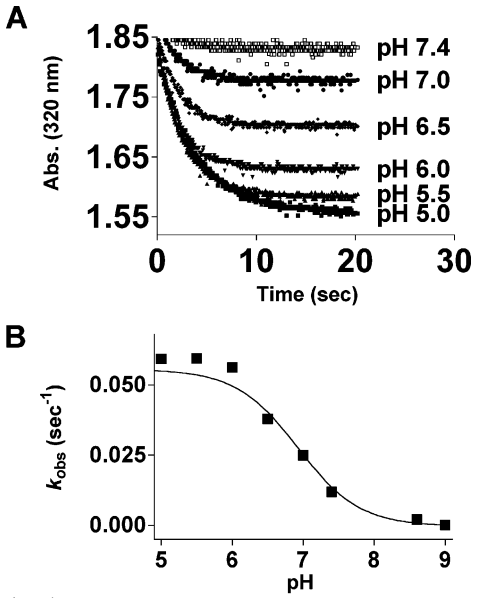

Figure 6. Stopped-flow determination of pK_a. N^2OPdG$^-$ (10^{-5} M final concentration) was combined with 0.25 M sodium phosphate buffer at neutral to basic pH to observe changes in the initial drop in absorbance at 320 nm (A). Initial rates from absorbance decay plots were used to determine the observed rate constants and plotted as a function of pH and fitted to a one-site binding function to yield a pK_a of 6.9 (B).

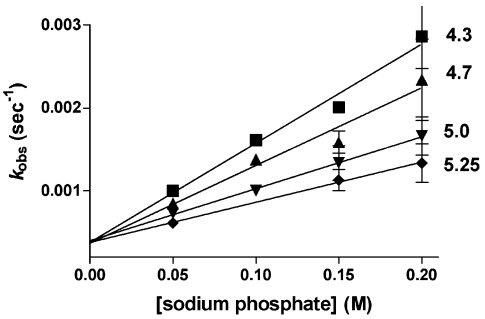

Figure 7. General-acid catalysis of N^2OPdG$^-$ ring-closure. Ring-closure to M_1dG was monitored by fluorescence increase with different concentrations of phosphate at various pH's. pH values are as follows: squares (■) 4.3; upward triangles (▲) 4.7; downward triangles (▼) 5.0; diamonds (◆) 5.25.

Table 3. Kinetic Constants for Ring-Closure in Nucleoside and Oligonucleotide at 25 °C[a]

substrate	$k_{cat.}$ (M^{-1} s^{-1})	$k_{uncat.}$ (s^{-1})	$k_{cat.}/k_{uncat.}$
N^2OPdG$^-$	106 ± 4.5	$(9.8 \pm 1.1) \times 10^{-4}$	10.8×10^4
AXA8mer	12.0 ± 0.8	$(5.0 \pm 0.2) \times 10^{-4}$	2.4×10^4
TXT8mer	20.2 ± 3.1	$(4.9 \pm 0.8) \times 10^{-4}$	4.1×10^4

[a] Substrates were combined with sodium phosphate buffers at various pH's to give final concentrations of 10^{-5} M and 0.25 M, respectively. Fluorescence increase plots were fit to a single-exponential increase to obtain k_{obsd}, and those values were plotted as a function of the concentration of H_3O^+ to give $k_{cat.}$ as a slope and $k_{uncat.}$ as the *y*-intercept.

protonated intermediate that has a reduced absorbance at 320 nm relative to M_1dG. Since the rate of protonated intermediate formation and ring-closure is small when N^2OPdG is an anion but enhanced when N^2OPdG$^-$ is placed under neutral and acidic conditions, the pK_a for N^2OPdG can be determined by measuring the rate of protonated intermediate formation at acidic pH.

Figure 6A shows the rapid phase of ring-closure over a wider range of pH values. Three phases are apparent from this plot: a phase where no drop in absorbance is observed, a phase where the equilibrium point is dependent upon the pH of solution, and a phase where the change in equilibrium point is constant regardless of pH. These absorbance decay plots were fit to linear functions to obtain initial rate constants for the formation of protonated intermediate (Equation 4). A plot of the initial rate constants of the rapid phase as a function of pH gives the pH titration curve (Figure 6B). The inflection point at pH 6.9 is the pK_a.

General-Acid Catalysis. General-acid catalysis was observed for the slow phase of the ring-closure reaction. The molar concentration of buffer used to induce protonation and ring-closure was varied, and the effects on k_{obsd} for fluorescence increase were determined. Figure 3B shows the rate of fluorescence increase was diminished based on the use of lower buffer concentrations. Similar effects were observed at variable buffer concentrations for the drop in absorbance upon acidification. These effects are represented graphically in Figure 7 as a plot of the concentration of buffer versus the observed rate constant for M_1dG formation. Using sodium phosphate buffers, the k_{obsd} for ring-closure by fluorescence detection was affected not only by pH of the buffer but also by the concentration of phosphate (or general acid) used. The slope of these plots yields the rate constant (k_{cat}) for acid catalysis of ring-closure. The nonzero *y*-intercept for these plots reveals that, at minimal concentration of general-acid, there is an uncatalyzed rate constant for ring-closure ($(3.7 \pm 0.2) \times 10^{-4}$ s^{-1}). This behavior is represented in the equation

$$k_{obsd} = k_{uncat} + k_{cat}[H_3O^+] \quad (5)$$

Experiments conducted to determine the effect of general acid on ring-closure of M_1dG in oligonucleotides are summarized in Table 3. As described for the monomer, the k_{cat} for ring-closure represents a significant increase in the rate constant for ring-closure of N^2OPdG$^-$ over the uncatalyzed rate constant. The extent of rate enhancement in the oligonucleotides is somewhat less than that observed with the mononucleoside.

Estimation of the pK_a of N^2OPdG by DFT Calculations. To corroborate the data above with a protonation event and anion stability, computational methods were used to probe changes in the pK_a of N^2OPdG relative to dG. Gradient-corrected density functional theory (DFT) calculations with the B3LYP functional were combined with the conductor-like polarizable continuum model (CPCM) to obtain solution-phase free energies in water. These were calculated for guanine, the N^2OPdG adduct, and the N1 and N^2 anions of each molecule. The results of the calculations are presented in Table 4. Structures and energies are provided in Supporting Information 2.

The gas-phase free energies of the ions show a substantial stabilization of the adduct anions at N1 or N^2 upon introduction of the oxopropenyl group at N^2. The gas-phase free energy of ionization at N^2 for guanine is 332.1 kcal/mol, but this decreases by 23.5 kcal/mol to 308.6 kcal/mol in N^2OPG. A similar but smaller effect is seen on ionization at the N1 position ($332.8-314.8 = 18$ kcal/mol). These differences are attenuated significantly in the solvent continuum to $22.6-14.9 = 7.7$ kcal/mol for N^2 and $21.3-15.5 = 5.8$ kcal/mol for N1.

The difference in the stabilities of the two N^2OPG ions is significant in the gas phase, where the N^2 anion is more stable

Table 4. Calculated pK_a for 9-Methyl-N^2OPG and 9-Methylguanine[a]

	G_{298}°(gas)	G_{298}° (H_2O)	ΔG_{298}° (gas)	ΔG_{298}° (H_2O)	pK_a	pK_{acorr}
9-Me-guanine	−581.941 193 1	−581.974 913 6				
9-Me-guanine (N1 anion)	−581.400 881 1	−581.510 281 8	332.8	21.3	15.6	9.4
9-Me-guanine (N^2 anion)	−581.401 985 3	−581.508 166 8	332.1	22.6	16.5	9.9
9-Me-N^2OPG	−772.686 303	−772.723 975 7				
9-Me-N^2OPG (N1 anion)	−772.174 581 6	−772.268 540 3	314.8	15.5	11.3	6.8
9-Me-N^2OPG (N^2 anion)	−772.184 441 9	−772.269 476 4	308.6	14.9	10.9	6.5

[a] Absolute free energies in hartree and free energies of deprotonation in kcal/mol.

than the N1 anion by 6.2 kcal/mol. This preference for ionization at N^2 is almost completely abolished in the solvent continuum where the two ions now only differ in free energy by 0.6 kcal/mol, with this small margin still favoring the N^2 ion. In the parent guanine, the N^2 ion is marginally more stable in the gas phase (0.7 kcal/mol), and preferential solvation of the N1 ion (of 2 kcal/mol) leads to its predominance at equilibrium.

The pK_a value calculated for guanine is 15.6. This is a substantial overestimation of the guanine pK_a relative to the experimental value of 9.2−9.6.[9] The calculated pK_a of N^2OPG is 10.9. This overestimation was expected based upon previous efforts to calculate solution phase pK_a's using continuum or self-consistent reaction field methods.[10−12] However, the data reflect stabilization of the anion by the oxopropenyl group and demonstrate the pK_a for N^2OPG is lower. If the error in the calculated pK_a is expected to be the same for both the guanine and N^2OPG anions based on errors in the solvation model, a scaling factor of 9.4/15.6 = 0.60 showing this error can be used. The pK_a for N^2OPG can be "corrected" in a manner similar to that applied by others to give a predicted pK_a of 6.8 for the N1 anion and 6.5 for the N^2 anion. The validity of these calculated pK_a's is supported by the pK_a determined from the spectroscopic data above. These values reflect a large decrease in the energy for ionization of the guanine ring upon N^2 substitution.

NMR Spectroscopy of Ring-Closure Intermediates. The biphasic kinetic data and the protonation data presented above suggest the formation of at least one intermediate beyond protonated N^2OPdG in the acid-catalyzed formation of M_1dG from N^2OPdG$^-$. NMR experiments were performed to find structural evidence for a primary intermediate that forms immediately after acidification, as well as to search for other intermediates that may form en route to M_1dG. N^2OPdG$^-$ was acidified at lower general-acid concentrations and at a lower temperature (0.05 M sodium phosphate, pH 5.0 at 8°C) than those described for the absorbance and fluorescence assays to decrease the rate constant of the ring-closure reaction to approximately 2.0×10^{-4} s^{-1}. One-dimensional ^{1}H NMR scans were taken at 60 s intervals. Experiments were performed using solvent suppression techniques to enhance sensitivity for important adduct proton resonances. Overlayed spectra ranging from 5.0 to 9.5 ppm are shown in Figure 8 (refer to the numbering scheme described in Figure 1 for proton assignments). Before acidification, only resonances corresponding to N^2OPdG$^-$ were observed[6] (trace A, Figure 8), and these shifted to resonances associated with two intermediates within 5 min of acidification (trace B, Figure 8). The H8 doublet resonance at 8.95 did not shift to a great extent, but the broad H6 multiplet at 8.3 ppm became a doublet at 8.0 ppm and H7 shifted downfield from under the solvent peak to 5.6 ppm. No chemical shifts unique to the N^2OPdG anion were observed once the solution was acidified, indicating the protonation was complete within the time scale of the first NMR experiment. Proton shifts corresponding to another intermediate (traces B through D, Figure 8) were observed as doublets at 6.45 and 6.55 ppm and a multiplet at 5.14 ppm, and new peaks for H1′ deoxyribose (6.0−6.3) and H2 of the purine ring (7.8−8.2) appeared. Finally, all intermediate protons disappeared at the final time point of 3 h to reveal exclusively M_1dG protons (trace E). Evaluations of the intensities of each resonance with respect to a DMF internal standard (7.8 ppm) revealed that both intermediates disappeared from solution at the same rate (see Supporting Information 3). The fact that neither intermediate dominated at any given time and that both disappeared to form M_1dG at the same rate implied the two forms were in rapid equilibrium, and the transition from the second intermediate to M_1dG was rate-limiting. These observations closely resemble those from the absorbance and fluorescence kinetic assays described above.

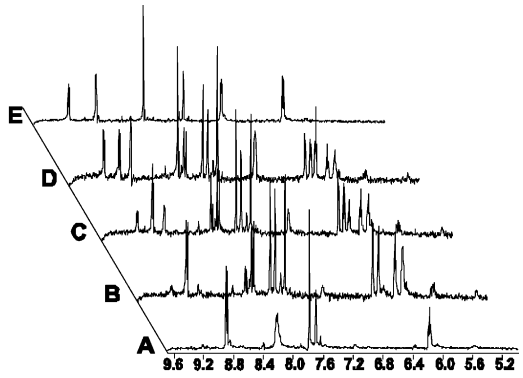

Figure 8. One-dimensional ^{1}H NMR spectra for acidified 10^{-3} M N^2OPdG$^-$ at 8 °C. One-dimensional spectra for acidified N^2OPdG$^-$ (10^{-3} M) were processed by XWIN-NMR and overlayed for comparison. (A) N^2OPdG$^-$ before acidification, (B) the acidified solution at 5 min, (C) the acidified solution at 1 h, (D) the acidified solution at 2 h, (E) the acidified solution at 3 h (M_1dG).

Though the 1D experiment described above provided strong evidence for the formation and disappearance of intermediates in an acidified solution of N^2OPdG$^-$, further work was necessary to evaluate coupling of intermediate proton resonances and determine structures for these intermediates. Figure 9 shows

(9) Singer, B.; Grunberger, D. *Molecular Biology of Mutagens and Carcinogens*; Plenum Press: New York, 1983.
(10) Klicic, J. J.; Friesner, R. A.; Shi-yi, L.; Guida, W. C. *J. Phys. Chem. A* **2002**, *106*.
(11) Jang, Y. H.; Sowers, L. C.; Cagin, T.; Goddard, W. A., III. *J. Phys. Chem. A* **2001**, *105*.
(12) Chipman, D. M. *J. Phys. Chem. A* **2002**, *106*.

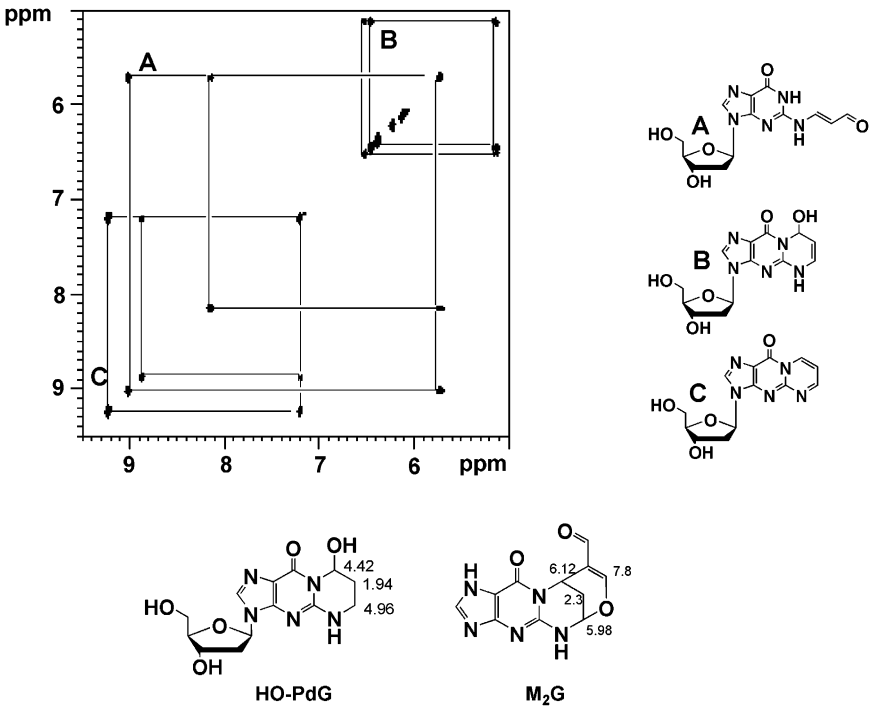

Figure 9. DQF-COSY for acidified 10^{-3} M N^2OPdG$^-$ 1 h after acidification. Two-dimensional spectra were processed by XWIN-NMR. Three distinct structures are observed in comparing the cross-peaks: (A) acidified N^2OPdG$^-$, (B) HO-Pr$_{ene}$-dG, and (C) M$_1$dG. Structures and important chemical shifts for related structures (HO-PdG and M$_2$G) are shown below.

the DQF-COSY spectrum of an acidified solution of N^2OPdG$^-$ that was acquired within 1 h of acidification. Three structures can be observed by analyzing the cross-peaks. The short dashed lines show cross-peaks for intermediate one (A), the protonated form of N^2OPdG. The cross-peak for 8.9 and 5.5 ppm ($^1J = 14$ Hz) is representative of the H8−H7 interaction, whereas the cross-peak for 5.5 and 8.2 ppm ($^1J = 10$ Hz) is the coupling for H7−H6 interactions. A second intermediate (B) is shown in the cross-peaks at 6.4 and 6.5 ppm (H8 and H6 respectively) with the intermediate H7 at 5.2 ppm ($^1J = 7$ Hz, 8 Hz). The solid line (C) for the cross-peak at 9.2 and 7.2 ppm is representative of the M$_1$dG H8−H7 interaction, indicating the presence of product.

The first intermediate is assigned as protonated N^2OPdG. The second intermediate is assigned as hydroxypropeno-dG (HO-Pr$_{ene}$-dG). This assignment is based on similar shifts observed for the structures for 8-hydroxypropano-dG (HO-PdG) and the dimeric MDA adduct of guanine, 9-formyl-6,10-methano-11-oxa-10*H*-[1,3,5]oxadiazocino[5,4-*a*]purine, M$_2$G (see Figure 9 for model structures and chemical shifts).[13] The similarity in the chemical environment for the H6 and H8 protons of HO-Pr$_{ene}$-dG and HO-PdG explains the trends in the chemical shifts and resonance couplings observed in this experiment. Data from Harris and co-workers on HO-PdG show that the H6 and H8 protons are nearly identical and contain an upfield shifted H7.[14,15] Introducing unsaturation about the C6−C7 bond in HO-Pr$_{ene}$-dG causes a general deshielding effect and the downfield shifts observed here. The carbinolamine proton of HO-Pr$_{ene}$-dG at H8, reported here at 6.3 ppm, is similar to that observed for M$_2$G which occurs at 5.98 ppm.

Ring-closure was also probed in a DNA duplex. Previous studies by Mao et al. have shown M$_1$G quantitatively ring-opens upon duplex annealing[16,17] and heating the duplex to 60 °C induces rapid denaturation and ring-closure. Although it was shown that ring-closure is rapid at this high temperature, the relative contributions of catalysis and elevated temperature to the rate of ring-closure are unknown because previous work has indicated that ring-opening and ring-closing are accelerated at high temperatures. To evaluate the time course for ring-closure at a lower temperature, a short sequence and its complement, both of which had been previously structurally characterized, were chosen to probe ring-closure by NMR. The melting temperature for the d(5′-GGTXTCCG:CCACAGGC-5′) (TXT:ACA) duplex has been reported to be approximately 20 °C and was easily denatured without heating to high temperature. The sample was prepared as described previously and maintained at neutral pH throughout the NMR experiements. One-dimensional ^{1}H NMR was completed for the duplex under native and denatured conditions. Figure 10 shows that, at 15 °C, the adduct is completely ring-opened in the duplex as evidenced by the absorbance of N^2OPdG at 8.9 ppm. The TXT:ACA duplex was rapidly warmed to 28 °C, and spectra were acquired immediately. After 200 s of data accumulation, the resonance for N^2OPdG in the duplex had completely disappeared, and two resonances for M$_1$dG H8 and H6 were apparent (9.0 and 9.2 ppm). The identity of these shifts was confirmed by 1H-COSY experiments and demonstrated the presence of

(13) Basu, A. K.; O'Hara, S. M.; Valladier, P.; Stone, K.; Mols, O.; Marnett, L. J. *Chem. Res. Toxicol.* **1988**, *1*, 53−59.
(14) Nechev, L. V.; Harris, C. M.; Harris, T. M. *Chem. Res. Toxicol.* **2000**, *13*, 421−429.
(15) Nechev, L. V.; Kozekov, I. D.; Brock, A. K.; Rizzo, C. J.; Harris, T. M. *Chem. Res. Toxicol.* **2002**, *15*, 607−613.
(16) Mao, H.; Reddy, G. R.; Marnett, L. J.; Stone, M. P. *Biochemistry* **1999**, *38*, 13491−13501.
(17) Mao, H.; Schnetz-Boutaud, N. C.; Weisenseel, J. P.; Marnett, L. J.; Stone, M. P. *Proc. Natl. Acad. Sci. U.S.A.* **1999**, *96*, 6615−6620.

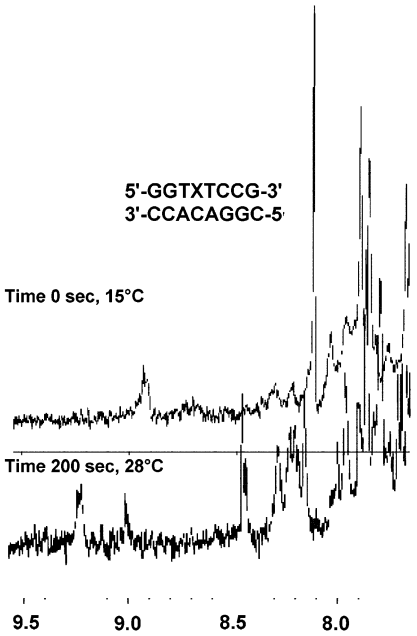

Figure 10. Proton NMR of double-stranded oligonucleotides before and after thermal denaturation. Lyophilized substrate duplex (5′-GGTXTCCG: 5′-CGGACACC) (TXT:ACA) was dissolved in 0.5 mL of buffer (0.05 M NaCl, 0.01 M Na H_2PO_4, and 5×10^{-4} M Na_2EDTA, pH 6.5) and proton NMR spectra were obtained over 200 s at 15 °C and 28 °C.

N^2OPdG and M_1dG at 15 °C and 28 °C, respectively (data not shown). More rapid data acquisition was attempted, but this was unsuccessful due to low sensitivity for the adduct resonance. When considering that the rate constants calculated for ring-closure of the single-stranded TXT 8mer near neutral pH are low, the fact that ring-closure happens so quickly in the denaturing duplex suggests that ring-closure is catalyzed during the process of denaturation.

Theoretical Studies of the Mechanism of N^2OPdG Ring-Closure. Based on the kinetic evaluation and NMR structural evidence above, theoretical calculations were performed to map a portion of the reaction coordinate for ring-closure from N^2-OPdG to form M_1dG. The potential energy surface is given in Figure 12, and the corresponding structures are shown in Figure 11. DFT was used to calculate gas-phase free energies and the CPCM to obtain solvation energetics. Relevant structures, electronic energies, thermochemical corrections, and solvation energies are included in the Supporting Information 4.

Starting with 9-methyl-(*E*)-N^2OPG, we examined the relative free energies of the different tautomeric forms that are likely to be present to some extent in the acidified solution: 9-methyl-(*E*)-N^2OPG (**1a**), its OPG-enol tautomer (**1b**), its O^6-enol tautomer (**1c**), and both OPG- and O^6-enol tautomers (**1d**). As expected, **1a** should be most abundant in solution based on these calculations. Enolization of the OPG moiety allows for rotation about the C6−C7 bond of the OPG group and, therefore, access to the 9-methyl-(*Z*)-N^2OPG with a barrier of 67 kJ/mol (**TS1**). This rotation is necessary for M_1dG formation as this is the configuration about the C6−C7 bond in the product. The energies of the various tautomers of (*Z*)-9-methyl-N^2OPG (**2a**−**d**) are shown. Again, the diketo tautomer (**2a**) should be most abundant in solution. The O^6-enol tautomer of (*Z*)-9-methyl-N^2OPG allows for ring-closure to form 9-methyl-HPG (**3**) via nucleophilic attack of N1 on the carbonyl of the oxopropenyl group concomitant with proton transfer from O^6 to the carbonyl oxygen (**TS2**). This occurs with a barrier of 68 kJ/mol from **2b**. If the 9-methyl-HO-Pr_{ene}-dG is protonated on the purine ketone (**3** + $\mathbf{H}^+$) and minimized to a transition state (**TS3**$^+$), the calculated energy is indicative of a smaller energy barrier to form products **4** + $\mathbf{H}^+$ and **4** than that observed for the previous two steps. This calculation suggests the final step is not rate-limiting, which is inconsistent with the findings of the NMR experiments performed with N^2OPdG$^-$ at pH 5. It is anticipated that the purine ketone of **3** has a very low pK_a, and only a trace amount would be protonated at neutral pH. However, the gas-phase techniques used for modeling the transition state are unable to model this concentration effect and are not reflective of the small concentration of proton donors (either hydronium or general acid) available to serve as catalysts at neutral pH. As a result, the calculated energy is more reflective of a case where all of the 9-methyl-HO-Pr_{ene}-dG is protonated. Since protonation is necessary for dehydration, the relatively slow rate of M_1dG formation observed at neutral pH is most likely due to the low basicity of HO-Pr_{ene}-dG.

Discussion

In the current study, ring-closure of N^2OPdG$^-$ in the nucleoside and in oligonucleotides was probed under acidic and neutral conditions. Based on the absorbance and fluorescence data as well as NMR structural studies, the following mechanism for ring closure is proposed (Figure 13). N^2OPdG$^-$ in the O^6 enol form **(1**$^-$**)** is first protonated to *E*-N^2OPdG-H (**1**). Tautomerization and rotation about the C6−C7 bond occur to give *Z*-N^2OPdG-H (**2**) as described in Figure 12. The oxopropenyl carbonyl is placed in proximity to N1 and results in nucleophilic attack on the carbonyl carbon and transfer of a proton to the carbonyl oxygen to yield HO-Pr_{ene}-dG (**3**). Up to this point, the events of ring-closure involve only the stoichiometric transfer of a proton to N^2OPdG$^-$. In contrast, the final and rate-limiting step in ring-closure involves the general-acid-catalyzed dehydration of HO-Pr_{ene}-dG. The proposed mechanism shows two likely paths to dehydration (**3A** and **3B**). Both pathways involve the formation of a cyclic enamine-imine structure that can originate from electron donation from either N^2 or N1 concerted with the elimination of water via protonation of the carbinolamine (**3**) by a general acid. The loss of water yields the resonance forms **4A** + $\mathbf{H}^+$ and **4B** + $\mathbf{H}^+$ that ultimately deprotonate to give the product M_1dG (**4**).

The model provided in Figure 13 is consistent with NMR data that show the presence of two distinct intermediates, N^2-OPdG-H and HO-Pr_{ene}-dG. Other intermediates proposed by this model are not observed presumably because they are present in too low a concentration or are converted to other intermediates too quickly to be observed on the NMR time scale. Although *Z*-N^2OPdG-H must be formed for cyclization to occur, it was not detected in the NMR experiments. The only doublet due to the H6 of N^2OPdG appeared to be due to the *E*-isomer.

Formation of HO-Pr_{ene}-dG is a reversible process that occurs prior to the rate-limiting step. Attack by the amide nitrogen occurs via the enol in a mechanism similar to that observed in aldol condensations.[18] The ease of this reaction is enhanced by the intramolecular transfer of the enol proton to the product HO-Pr_{ene}-dG. It is of note that the cyclization leads to the

(18) Carey, F. A.; Sundberg, R. J. *Advanced Organic Chemistry*, 3rd ed.; Plenum Press: New York, 1990.

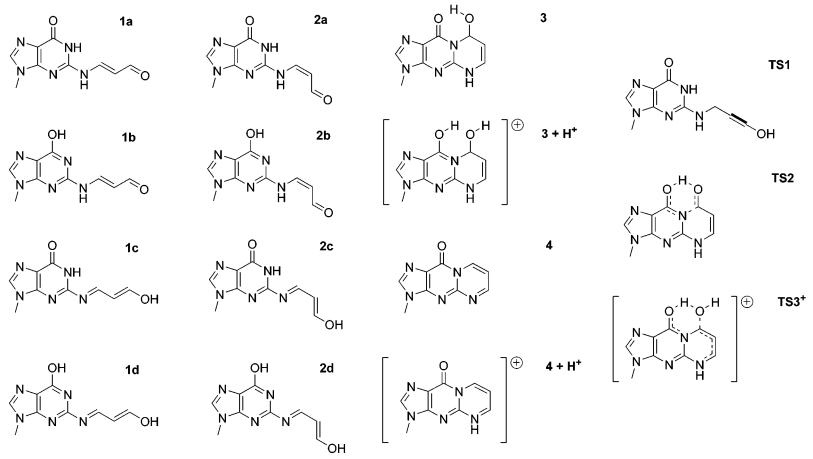

Figure 11. Structures for DFT-calculated intermediates to N^2OPG$^-$ ring-closure.

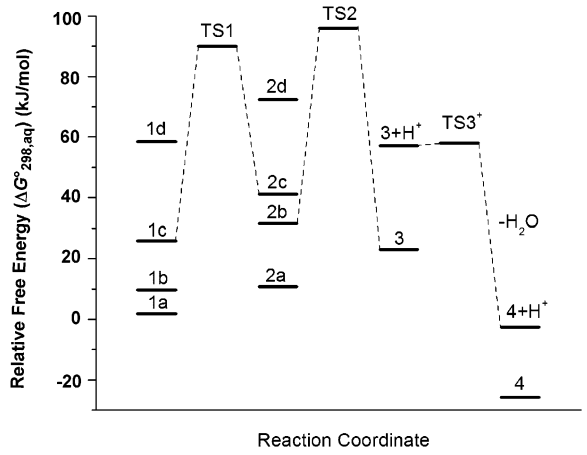

Figure 12. Energy surface for DFT-calculated intermediates. Lines connecting energy levels show those structures believed to be involved in the mechanism of ring-closure.

formation of a stereocenter at the resulting carbinolamine carbon of HO-Pr$_{ene}$-dG. However, the rate data described in this study do not allow for distinguishing the rates of the formation or dehydration for the two carbinolamine diastereomers, nor is there any observable NMR resolution in our experiments of diastereomeric protons.

DFT calculations were completed to predict likely structures formed en route to ring-closure. The reaction coordinate shown in Figure 12 that predicts rotation of *E*- and *Z*-N^2OPdG-H and the ring-closure of the *Z* form to HO-Pr$_{ene}$-dG represent the main energy barriers to ring-closure. Dehydration has a lower energy barrier. As discussed above, modeling of the dehydration was complicated by the fact that explicit protonation was required, which is inconsistent with the low pK_a anticipated for the protonated HO-Pr$_{ene}$-dG. When considering the concentration of catalyst necessary for dehydration to occur, the energy barrier for the elimination of water at neutral pH is expected to be much higher than that drawn in Figure 12, which explains why dehydration is rate-limiting and general-acid catalyzed. Slow rates of dehydration in other pyrimidinol/pyrimidone systems have been observed[19,20] as well as for other unsaturated carbinolamines.[21−23]

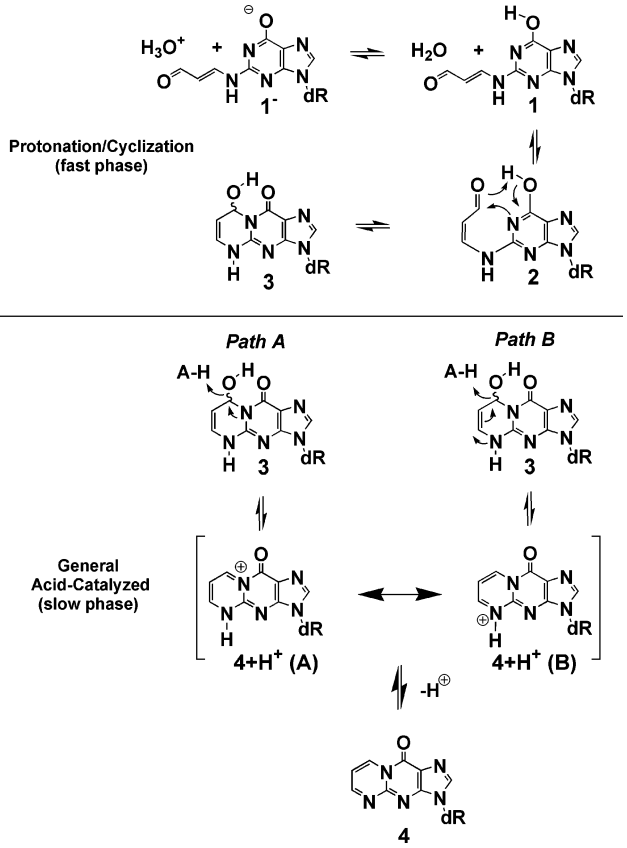

Figure 13. Proposed mechanism of ring-closure.

Catalyzed and uncatalyzed steps in the sequence of reactions shown in Figure 13 are observed as a biphasic reaction. The events preceding the dehydration step occur by the stoichiometric addition of a proton to N^2OPdG$^-$ and following cyclization, dehydration is general-acid-catalyzed. These two distinct phases are demonstrated by both absorbance and fluorescence spectroscopy. Initial protonation of N^2OPdG$^-$ to a neutral species establishes an equilibrium between protonated N^2OPdG and HO-Pr$_{ene}$-dG prior to dehydration to M$_1$dG. This equilibrium between intermediates is observed by NMR spectroscopy, where proton resonances from both compounds disappear at the same

(19) Nolan Carter, K.; Greenberg, M. M. *Bioorg. Med. Chem.* **2001**, *9*, 2341−2346.
(20) O'Donnell, R. E.; Boorstein, R. J.; Cunningham, R. P.; Teebor, G. W. *Biochemistry* **1994**, *33*, 9875−9880.
(21) Keys, L. D.; Hamilton, G. A. *J. Am. Chem. Soc.* **1987**, *109*, 2156−2163.
(22) Palmer, J. L.; Jencks, W. P. *J. Am. Chem. Soc.* **1980**, *102*, 6466−6472.
(23) Llor, J.; Asensio, S.; Sanchez-Ruiz, J. *Int. J. Kin.* **1989**, *21*, 51−61.

rate (Supporting Information 2). This explains why the NMR resonance for *E*-N^2OPdG-H does not decrease to zero initially and why both intermediates are detectable until only M_1dG remains. The fact that this equilibrium is established rapidly is supported by the fact that the increase in fluorescence attributed to M_1dG, the only fluorescent species in the proposed model, begins to occur at the conclusion of the fast phase and indicates some HO-Pr_{ene}-dG has formed by the end of the fast phase. N^2OPdG-H and HO-Pr_{ene}-dG are both expected to absorb less than the ring-opened anion due to loss of the anion charge and conjugation, respectively. This dependence on protonation has been observed for guanine and malondialdehyde, and Supporting Information demonstrates protonation of N^2OPdG$^-$ at pH 6.5 causes a shift in the guanine absorption band from 260 to 252 nm (Supporting Information 5).

Fast phase / Slow phase

$$N^2\text{OPdG}^- + H_3O^+ \underset{K_a}{\rightleftharpoons} N^2\text{OPdG-H} + H_2O \rightleftharpoons \text{HO-Pr}_{ene}\text{-dG} \overset{\text{HA (cat.)}}{\rightleftharpoons} M_1\text{dG} \quad (6)$$

Dehydration is slow and results in the final decrease in absorbance at 320 nm and conversion to the fluorescent product.

The differences in the plots observed for UV and fluorescence change allow for further characterization of this model. The concentration of acid in solution positively affected the rate of both the fast and slow phases of ring-closure, and no ring-closure was observable in this assay at pH values greater than 8.6. The role of acid in both phases of ring-closure was found to be different. During the fast phase, acid was observed as a reactant. The position of the plateau in the drop of A_{320} was demonstrated to be dependent on the pH. The fast phase was also shown to be a combination of protonation and adduct rearrangement and could be extended to longer times by cooling (Supporting Information 1). The pK_a was determined from a plot of k_{obsd} for the fast phase versus pH, giving an inflection point and a value of pK_a of 6.8. The fact that the pK_a is three units lower than the pK_a of N1 of deoxyguanosine (ca. 10) was supported by DFT calculations for the free energies of protonated and deprotonated 9-methyl-N^2OPG, which also predict a lower pK_a for N1. These results together suggest the oxopropenyl group of N^2OPG provides 1000-fold stabilization for developing anions on the purine ring.

In contrast to the kinetics of the fast phase, absorbance decay and fluorescence increase were both shown to be affected by pH and buffer concentration. Despite the fact that the slow phase of ring-closure could be accelerated at lower pH and higher buffer concentration, the endpoint of the slow phase was the same. This observation is consistent with general-acid catalysis. Based on the model suggested in Figure 13, catalysis was related to dehydration because it is the rate-limiting step. An uncatalyzed rate of ring-closure could be obtained by comparing the rate constants for ring closure at different concentrations of general acid and pH (Figure 7).

It is of note that the unimolecular rate constant for uncatalyzed ring-closure (3.7×10^{-4} s^{-1}) measured in this paper is similar to that observed in a previous study where the reverse rate constant to ring-opening at basic pH was 1.7×10^{-4} s^{-1}.[7] There is an important distinction between the dehydration reaction observed at acidic and basic pH and relates to the protonation state of HO-Pr_{ene}-dG. Ring-closure of the anionic species results in the formation of anionic HO-Pr_{ene}-dG and elimination of hydroxide, whereas the reaction in this study involves a neutral HO-Pr_{ene}-dG becoming protonated and eliminating water. As discussed above, the pK_a for HO-Pr_{ene}-dG is predicted to be much lower than 7.0 and is the key factor in the slow-rate constants for dehydration and M_1dG formation observed at neutral pH. As a result, dehydration of neutral HO-Pr_{ene}-dG is slow and requires protonation, whereas dehydration of the anion of HO-Pr_{ene}-dG is facilitated by the elimination of a negative charge by the expulsion of hydroxide.

Catalysis in ring-closure was also studied in duplex DNA where N^2OPdG was placed opposite dC in the complement. Previous reports showed that denaturation and heating to 60 °C resulted in ring-closure to M_1dG.[17] One-dimensional proton NMR at a lower temperature (28 °C) and at pH 6.5 demonstrated quantitative ring-closure upon duplex denaturation at the first time point practically achievable (200 s). Based on the k_{obsd} at 25 °C determined in single-stranded DNA, the rate of ring-closure in the denatured duplex is over 100-fold faster at much lower concentration of general acid. This rate enhancement for ring-closure when compared to the single-stranded adduct is too large to be explained only by the modest increase in temperature used to denature the strands in our duplex study (15 °C to 28 °C). Based on previous results by Mao and coworkers,[16,17] stabilization of the oxopropenyl group of N^2OPdG is provided by the adduct projecting into the minor groove of the duplex, shielding it from interacting with the nucleophilic site at N1. This conformation for N^2OPdG must then quickly change when the duplex denatures, enabling ring-closure. One possible explanation for the acceleration provided by the duplex is the fact that the adduct is fully protonated and exists as a neutral species in duplex DNA. When considering this fact, ring-closure to HO-Pr_{ene}-dG should proceed rapidly upon melting the duplex. However, it is not known how the presence of the complementary strand accelerates dehydration of HO-Pr_{ene}-dG over that observed in the single strand.

The findings reported in this and another recent article provide a comprehensive picture of the chemistry of interconversion of M_1dG and N^2-OPdG from pH 4−12. At low-to-neutral pH, M_1-dG predominates by virtue of the facile ring closure of N^2OPdG to HO-Pr_{ene}-dG and its subsequent elimination of water. Dehydration is the rate-limiting step in the conversion of N^2-OPdG to M_1G and is subject to general-acid catalysis. At basic pH, the anion of N^2OPdG is formed by reversible addition of hydroxide to M_1dG. A critical determinant of the chemistry of ring-opening and -closing is the acidity of N^2OPdG. Experimental and theoretical determinations indicate that substitution of the oxopropenyl group on N^2 of deoxyguanosine lowers the pK_a of the imino proton by approximately 3 orders of magnitude to a value of 6.8. The protonated form of N^2OPdG is subject to ring-closure to HO-Pr_{ene}-dG (likely mediated by tautomerization and isomerization), whereas the deprotonated form is not. Thus, at basic pH's, N^2OPdG accumulates. A corollary of this finding is that the aldehyde of N^2OPdG is much less reactive to nucleophiles at neutral-to-basic pH than at acidic pH.

These studies also provide insight into the role of duplex DNA in the catalysis of ring-opening of M_1dG and ring-closing of N^2OPdG. Ring-opening is catalyzed by deoxycytidine-mediated hydroxide attack on C-8 of M_1dG in the approaching comple-

mentary strand. Stabilization of N^2OPdG (perhaps the protonated form) is driven by annealing of the duplex, which places N^2-OPdG in the minor groove, where it cannot attack N1 to initiate cyclization. If N^2OPdG is protonated, its aldehyde group would be reactive to externally added nucleophiles. On denaturation of duplex DNA, N^2OPdG cyclizes to M_1dG at a rate much higher than that observed in single-stranded DNA. The duplex structure must catalyze dehydration of HO-Pr_{ene}-dG since this is the rate-limiting step in the conversion of N^2OPdG to M_1dG.

Experimental Section

Materials. All materials were obtained from commercial sources unless otherwise noted. M_1dG was synthesized as previously described.[24] Oligonucleotides containing the MDA-dG adduct (AXA 8mer, 5′-GGAXACCG-3′; TXT 8mer, 5′-GGTXTCCG-3′; X is M_1dG at pH 7.4) were synthesized as reported elsewhere.[24] Complimentary oligonucleotide (5′-CGGACACC-3′) was obtained from Midland Certified Reagent Company (Midland, TX). Solutions of N^2OPdG$^-$ or N^2OPG$^-$ containing oligonucleotide were generated directly before use by combining concentrated M_1dG with 0.050 M sodium phosphate, pH 11.2. After sitting for 30 min at ambient temperature, the concentrated N^2OPdG$^-$ solution was diluted to the desired concentration.

Ring-Closure Assay. Ring closure was monitored using the HP 845X UV spectrometer with temperature control. N^2OPdG$^-$ was diluted to a final concentration of 1.0×10^{-5} M in 10^{-4} L. Experiments were initiated by acid treatment with sodium phosphate buffer solutions at various pH's and concentration. Changes in the absorbance at 320 nm or in fluorescence at 511 nm (excitation at 363 nm) were observed over time until the reaction reached completion. Experiments were done in duplicate, and the decay plots were averaged. The resultant plots were fitted to a one-phase exponential decrease function using GraphPad Prism to obtain k_{obsd} values.

Ring-Closure Assay (Stopped-Flow). Stopped-flow measurements for ring-closure were carried out with conditions exactly as those described above for the ring-closure assay except for the use of a stopped-flow spectrophometer (Applied Photophysics, Leatherhead, UK). Monochromators in series were used with slit widths set to 5 and 10 mm to obtain maximal signal. Measurements were made from 1 to 200 s (collecting 1000 data points). For the most part, the reaction was completed within 20 s. Changes in the absorbance at 320 nm were observed over time and then fitted to one-phase exponential decrease functions using GraphPad Prism software.

NMR Spectroscopy on N^2OPdG$^-$. Proton NMR and double quantum filtered correlation spectroscopy (DQF-COSY) experiments were performed on Bruker DRX 500 or DRX 600 MHz instruments. Data were processed using XWIN-NMR. All NMR studies were done with samples in D_2O. Water signals were suppressed for both experiments using watergate solvent suppression techniques in order to observe exchangeable protons.[25] Chemical shifts were referenced in proton spectra using the aldehydic peak of *N*,*N*-dimethylformamide (7.91) as an internal standard. Chemical shifts in the DQF-COSY experiments were referenced to the shift of water (4.7).

NMR Spectroscopy on Duplex Oligonucleotide Containing N^2OPdG. The NMR sample of ds TXT:ACA was prepared by combining TXT 8mer with its complementary sequence in 0.5 mL of buffer (0.05 M NaCl, 0.01 M Na H_2PO_4, and 5×10^{-4} M Na_2EDTA, pH 6.5) to a final concentration of 5×10^{-4} M duplex oligonucleotide. The sample was exchanged with 99.96% D_2O several times to eliminate water. Experiments were performed at 400.13 MHz using a Bruker DRX spectrometer. Using a watergate suppression pulse sequence,[25] the proton spectrum of the annealed duplex was determined at 15 °C. To evaluate ring-closure upon duplex denaturation, the sample was rapidly heated to 28 °C to melt the duplex and data were accumulated immediately. Data were accumulated at 200 s intervals for 10 min and were processed using XWIN-NMR. All spectra are referenced to the chemical shift of water (4.7).

Computational Methods. Calculations were performed using the Gaussian 98 suite of programs compiled to run on an SGI Origin.[26] A model for N^2OPdG$^-$, 9-methyl-N^2OPG, was used instead of the full nucleoside in order to minimize computational expense. Generalized gradient density functional theory was used to optimize the structures and calculate vibrational frequencies using the B3LYP exchange-correlation functional along with a 6-31G(d) basis set.[28] Following gas-phase minimizations and vibrational frequency calculations, single-point energy calculations were performed with a larger 6-311+G-(2d,2p) basis set. This provided electronic energies that were corrected to free energies at 298 K using the scaled (by 0.9806) thermochemical corrections from the smaller basis calculations.[29] Free energies in water were obtained by adding solvation energies calculated using the CPCM solvation model of Barone and Cossi to the gas-phase free energies.[30] The pK_a values were determined by calculating the free energy change for the following deprotonation reaction:

$$9\text{-Me-}N^2\text{OPG} \rightarrow (9\text{-Me-}N^2\text{OPG})^- + H^+ \qquad (7)$$

and the pK_a calculated from the free energy change by

$$pK_a = -\Delta G/2.303RT \qquad (8)$$

The free energy of a proton in water (−270.3 kcal/mol) is obtained by combining the gas-phase free energy of a proton ($2.5RT - T\Delta S^\circ$ = −6.3 kcal/mol) with the solvation energy of a proton in water (−264 kcal/mol), which was taken from the recent work by Tissandier et al.[31] Since it is well-known that the self-consistent reaction fields employed in simulating solvent effects severely underestimate the solvation energies of many ions, we have also calculated the pK_a in guanine and, based upon the difference from the experimental value (9.2−9.6), scaled our calculated pK_a for N^2OPG accordingly. This is related to virtually all recent pK_a calculations, which use some sort of overall multiplicative scaling of the calculated pK_a.

The reaction coordinate for ring-closure was studied using the same theoretical methodology. Stationary points were characterized as either minima or saddle points depending on the outcome of the normal-mode analysis in whether 0 or 1 imaginary frequencies existed, respectively.

Acknowledgment. This research was supported by research and center grants from the National Institutes of Health (CA87819 and ES-00267). J.N.R. was supported by a training grant (ES07028). D.A.P. would like to thank N. A. Porter, Vanderbilt University, and NSERC Canada for support. We are grateful to J. Smith and the Vanderbilt Center for Structural Biology for generous access to computational resources and NMR instrumentation, to Y. J. Cho for his help in NMR

(24) Schnetz-Boutaud, N. C.; Mao, H.; Stone, M. P.; Marnett, L. J. *Chem. Res. Toxicol.* **2000**, *13*, 90−95.
(25) Piotto, M.; Saudek, V.; Sklenar, V. *J. Biomol. NMR* **1992**, *2*, 661−665.
(26) Frish, M. J.; Trucks, G. W.; Schlegel, H. B.; Scuseria, G. E.; Robb, M. A.; Cheeseman, J. R.; Zakrzewski, V. G.; Montgomery, J. A.; Stratman, R. E.; Burant, J. C.; Dapprich, S.; Millam, J. M.; Daniels, A. D.; Kudin, K. N.; Strain, M.; Farcas, O.; Tomasi, J.; Barone, V.; Cossi, M.; Cammi, R.; Mennucci, B.; Pomelli, C.; Adama, C.; Clifford, S.; Oschterski, J.; Petersson, G. A.; Ayala, P. Y.; Cui, Q.; Morokuma, K.; Malick, D. K.; Rabuck, A. D.; Raghavachari, K.; Roesman, J. B.; Cioslowki, J.; Ortiz, J. V.; Stefanov, B. B.; Liu, G.; Liashenko, A.; Piskorz, P.; Komaromi, I.; Gomperts, R.; Martin, R. L.; Fox, D. J.; Keith, T.; Al-Laham, M. A.; Peng, C. Y.; Nanayakkara, A.; Gonzalez, C.; Callacombe, M.; Gill, P.; Johnson, B. G.; Chen, W.; Wong, M. W.; Andres, J. L.; Head-Gordon, M.; Replogle, E. S.; Pople, J. A. *Gaussian 98*; Gaussian, Inc.: Pittsburgh, PA, 1998.
(27) Reference deleted after ASAP publication.
(28) Becke, A. D. *J. Chem. Phys.* **1993**, *98*, 5648.
(29) Scott, A. P.; Random, L. *J. Phys. Chem. A* **1996**, *100*, 16502−16513.
(30) Barone, V.; Cossi, M. *J. Phys. Chem. A* **1998**, *102*, 1995−2001.
(31) Tissander, M. D.; Cowen, K. A.; Feng, W. Y.; Gundlach, E.; Cohen, M. H.; Earhart, A. D.; Coe, J. V. *J. Phys. Chem. A* **1998**, *102*.

experimentation, and to R. N. Armstrong for access to the stopped-flow spectrophotometer.

Note Added after ASAP Posting. After this paper was posted ASAP on July 24, 2004, several errors were discoverd. Typographical errors in the title have been corrected; ref 7 has been expanded; a minus sign has been added to indicate the anion in line 7 of the first paragraph of the Results section; the column 1 headings for Tables 1 and 2, the first line of the Figure 5 caption, and the units in the Table 4 footnote have been corrected; structural changes have been made in Figure 11; the sentence begining "As discussed above..." has been revised in the full paragraph under Figure 12; the value in the first line under eq 8 has been corrected; and ref 27 has been deleted. The corrected version was posted August 4, 2004.

Supporting Information Available: Figures depicting delayed fast-phase of reactions, parallel kinetics of disappearance of intermediate protons, and hypsochromic shift in absorbance spectrum of N^2-OPdG on protonation. Calculated energies of deprotonated N1 and N^2 and of intermediates in ring-closing. This material is available free of charge via the Internet at http://pubs.acs.org.

JA040010Q